Substrate specificity and subsite mobility in *T. aurantiacus* xylanase 10A

Leila Lo Leggio[a,*], Stavros Kalogiannis[b], Kelvin Eckert[a,c], Susana C.M. Teixeira[d],
Mahalingeswara K. Bhat[e], Carmen Andrei[a,f], Richard W. Pickersgill[g], Sine Larsen[a]

[a]*Centre for Crystallographic Studies, Chemical Institute, University of Copenhagen, Universitetsparken 5, DK-2100 Copenhagen, Denmark*
[b]*Hellenic Sugar Industry S.A., Agricultural Research Centre, Laboratory of Industrial Microbiology, Thessaloniki, Greece*
[c]*Humboldt Universität Berlin, Institute of Biology, Department of Bacterial Physiology, Chausseestr. 117, 10115 Berlin, Germany*
[d]*Chemistry Department, University of Reading, Whiteknights, Reading RG6 6AD, UK*
[e]*Institute of Food Research, Norwich Research Park, Colney Lane, Norwich NR4 7UA, UK*
[f]*Department of Physics, 'Babes-Bolyai' University, Faculty of Physics, M. Kogàlniceanu No. 1, 3400 Cluj-Napoca, Romania*
[g]*Biological Sciences, Medical Science Building, Queen Mary University of London, London E1 4NS, UK*

Abstract The substrate specificity of *Thermoascus aurantiacus* xylanase 10A (TAX) has been investigated both biochemically and structurally. High resolution crystallographic analyses at 291 K and 100 K of TAX complexes with xylobiose show that the ligand is in its α anomeric conformation and provide a rationale for specificity on *p*-nitrophenyl glycosides at the -1 and -2 subsites. Trp 275, which is disordered in uncomplexed structures, is stabilised by its interaction with xylobiose. Two structural subsets in family 10 are identified, which differ by the presence or absence of a short helical stretch in the eighth $\beta\alpha$-loop of the TIM barrel, the loop bearing Trp 275. This structural difference is discussed in the context of Trp 275 mobility and xylanase function. © 2001 Federation of European Biochemical Societies. Published by Elsevier Science B.V. All rights reserved.

Key words: Family 10; Tryptophan; Enzyme–substrate complex; Glycerol; Specificity; Glycoside hydrolase

1. Introduction

Xylanases hydrolyse internal β-1,4 bonds in the main chain of xylan, a major polysaccharide constituent of the plant cell wall. Their biotechnological applications range from chlorine-free paper bleaching to use as food and animal feed additives. The thermophilic fungus *Thermoascus aurantiacus* produces a major xylanase, xylanase 10A (TAX), previously referred to as xylanase I [1]. The three-dimensional structure of TAX has been determined by us to 1.14 Å resolution [2,3] and independently to 1.8 Å resolution [4].

TAX belongs to family 10 in the classification of glycoside hydrolases [5], for which structures of several other members are also available [6–12]. Family 10 in turn belongs to the 4/7 superfamily of TIM barrels (also known as clan GH-A)

[13,14] which includes glycoside hydrolases with similar architecture and conserved mechanism, but diverse specificities. Family 10 enzymes retain the configuration at the anomeric carbon via a double displacement mechanism involving two glutamates, one functioning as acid/base and one functioning as nucleophile [15]. Three conserved tryptophans form an aromatic cage around subsite -1 (Trp 87, Trp 267 and Trp 275 in the TAX numbering), and have been shown to be important for enzyme function by mutation studies [16–18]. Trp 275 in particular has been implicated in substrate specificity [19,20] and is a signature residue in family 10, as none of the other 4/7 superfamily enzymes have an equivalent aromatic residue. In this study we further investigate the structure–function relationship of substrate specificity in family 10, taking TAX as a starting point.

2. Materials and methods

2.1. Xylanase purification and assay

TAX was purified as previously described [21]. Activity towards polysaccharides was measured by the dinitrosalicylic acid assay [22] in 50 mM sodium citrate buffer pH 5.3 at 50°C. *p*-Nitrophenyl (pNP) glycoside hydrolysis was assayed in microtitre plates by measuring the change in absorbance at 410 nm after addition of excess Na_2CO_3.

2.2. Crystallographic methods

TAX crystals were prepared as previously described [2] and were isomorphous to crystal form II (space group P2$_1$, $a = 46.22$ Å, $b = 59.24$ Å, $c = 51.31$ Å, $\beta = 109.8°$). The TAX structure in complex with xylobiose collected at room temperature (XBRT) data were collected to 1.8 Å resolution at room temperature from a crystal soaked for 45 min in 0.5 M xylobiose, 25% polyethylene glycol 6000. The TAX structure in complex with xylobiose collected at cryogenic temperature (XBCRYO) data were collected at 100 K to 1.7 Å resolution from a crystal soaked for a few minutes in a mother liquor solution containing 25% glycerol and 0.5 M xylobiose and then flash cooled. The TAX structure in complex with glycerol collected at cryogenic temperature (GLC) data were collected at 100 K to 1.87 Å resolution from a crystal flash cooled in 0.125 M Na-citrate buffer pH 5.6, 12.5% glycerol and 0.15 M maltoheptaose.

Data were collected using CuKα radiation from a rotating anode generator (XBRT and GLC) or using synchrotron radiation at Elettra (XBCRYO) and processed with Denzo/Scalepack [23]. All data sets had more than 50% reflections with $I/\sigma > 2$ in the outer resolution shell. The structures were refined with XPLOR 3.851 [24] (XBRT) or CNS 0.9 [25] (XBCRYO and GLC) and rebuilt using O [26]. Selected statistics are shown in Table 1. Further crystallographic details can be found in the PDB depositions (codes 1GOQ for XBRT, 1GOR for XBCRYO and 1GOO for GLC). Revised versions of the original structure determinations have PDB codes 1K6A, 1GOK, 1GOM.

---

*Corresponding author. Fax: (45)-35320299.
E-mail address: leila@ccs.ki.ku.dk (L. Lo Leggio).

Abbreviations: TAX, *Thermoascus aurantiacus* xylanase I; GLC, TAX structure in complex with glycerol collected at cryogenic temperature; XBRT, TAX structure in complex with xylobiose collected at room temperature; XBCRYO, TAX structure in complex with xylobiose collected at cryogenic temperature; CEX, xylanase/exocellulase Cex from *Clostridium fimi*; CMC, carboxymethylcellulose; pNP, *p*-nitrophenyl; RSCC, real space correlation coefficient calculated in CNS against a Sigmaa $2F_{obs} - F_{calc}$ map

Table 1
Selected statistics for the structures of TAX in complex with xylobiose and glycerol

	XBRT	XBCRYO	GLC
Completeness (%)	86	95	99.7
R_{sym} (%)	17.0	6.3	6.4
R_{sym} (%) (in outer resolution shell)	33.8 (1.83–1.80 Å)	34.3 (1.76–1.70 Å)	31.5 (1.90–1.87 Å)
Redundancy	6.4	2.8	3.2
Final R-factor (%)	16.7	17.4	17.5
Final R-free (%)	21.2	20.0	20.7

3. Results

3.1. Substrate specificity of TAX

TAX kinetic parameters were determined for different poly-saccharides: $K_M = 3.3$ mg/ml and $k_{cat} = 350$ s^{-1} for birchwood xylan (Sigma); $K_M = 3.1$ mg/ml and $k_{cat} = 319$ s^{-1} for birchwood xylan (Roth); $K_M = 2.6$ mg/ml and $k_{cat} = 273$ s^{-1} for glucuronoxylan; $K_M = 3.3$ mg/ml and $k_{cat} = 350$ s^{-1} for oat spelt xylan (soluble fraction). No activity was detected for Avicel and carboxymethylcellulose (CMC). Barley glucan could be hydrolysed to some extent, but the activity was not linearly dependent on enzyme concentration, so that kinetic parameters could not be determined. TAX was also tested for activity on several pNP derivatives of mono- and disaccharides, as shown in Table 2.

3.2. TAX complexes with xylobiose

The protein portions of the native and complexed structures of TAX are very similar. In both xylobiose complexes, XBRT (long soak followed by room temperature data collection) and XBCRYO (short soak followed by data collection at cryogenic temperatures), xylobiose bound to subsites −2 and −1. 'Minus' subsites indicate the non-reducing end of a substrate spanning the substrate binding groove, 'plus' subsites the reducing end, counting from the scissile bond [27]. In the XBRT structure there is also evidence for extra xylose moieties occupying subsite +1 (Fig. 1a,c) and two other sites far from the active site (not shown), presumably as a consequence of the longer soaking time.

All xylose moieties have been modelled into the electron density in their $^4C_1$ chair conformation. The xylose moiety at subsite −1 is poorly defined in the XBRT electron density maps, whereas the Fourier difference map for the XBCRYO structure prior to incorporation of xylobiose in the model is of excellent quality (Fig. 1b). This structure represents a substantial improvement in resolution over the best non-covalent family 10 complexes previously obtained with unmodified xylooligosaccharides [28]. The increased resolution shows that the xylose moiety at subsite −1 is best modelled as its α anomer, with the anomeric oxygen 2.39 Å away from the catalytic nucleophile. The β anomer would result in a short contact with the acid base if the xylose ring were in an equivalent position. This may be a mechanism by which substrate distortion from the $^4C_1$ conformation is initiated during catalysis, and a reason why sugar moieties at subsite −1 tend to be disordered [29]. TAX apparently selects for the anomeric form that most closely resembles the covalent intermediate.

The enzyme–xylobiose interactions at subsites −2 and −1 in XBRT and XBCRYO (Fig. 1a) are similar to the ones previously reported for covalent [19,20,30,31] and non-covalent [28,32,33] enzyme–ligand complexes of family 10 en-zymes. All protein residues involved in interactions at subsites −2 and −1 are conserved within family 10.

In neither the XBRT nor XBCRYO models is there evidence of a 180° rotation of the xylosyl moiety at the −2 subsite as reported for the complex of *Penicillium simplicissimum* xylanase with xylobiose [28], but not for its complexes with xylotriose, xylotetraose or xylopentaose (Fig. 1b). The xylose ring at subsite −1 is shifted further away from the catalytic nucleophile in the TAX complexes compared to the covalent complexes [19,20,30,31] and also to the non-covalent complexes with xylobiose-derived inhibitors [33], which lack the anomeric hydroxyl group. His 209 interacts with the anomeric oxygen at subsite −1 in its α conformation. At subsite +1, O1 of xylose is interacting with a water molecule absent in the uncomplexed structures, while O2 and O3 are hydrogen-bonded to the side chain of Lys 120 of a symmetry-related molecule. O4 is in close contact to the catalytic acid base, Glu 131. The xylose ring is sandwiched between the conserved residues Tyr 174 and Trp 275, so that Tyr 174 fulfils a similar role to Phe 181 in *Pseudomonas fluorescens* xylanase 10A complexed with xylopentaose [32], where the xylosyl unit at subsite +1 displays a similar binding mode (Fig. 1c). In the *P. simplicissimum* xylanase complexes [28], binding in the plus side of the substrate binding groove is not in an equivalent position (Fig. 1c).

3.3. Glycerol mimics xylobiose at subsite −1

A glycerol molecule originating from the cryoprotectant was localised at subsite −1 in the active site of the cryocooled

Table 2
TAX specific activity on pNP-glycosides (2.5 mM)

Substrate	Activity (U/mg)
Pentose monosaccharide derivatives	
pNP-β-D-xylopyranoside	60.6
pNP-α-D-xylopyranoside	–
pNP-α-L-arabinofuranoside	121.7
pNP-α-L-arabinopyranoside	161.9
pNP-α-L-arabinopyranoside	–
Hexose monosaccharide derivatives	
pNP-β-D-glucopyranoside	12.7
pNP-α-D-glucopyranoside	–
pNP-β-D-glucuronoside	–
pNP-β-D-galactopyranoside	15.7
pNP-α-D-galactopyranoside	–
pNP-β-D-mannopyranoside	–
pNP-α-D-mannopyranoside	–
Disaccharide derivatives	
pNP-β-D-cellobioside	1296.1
pNP-β-D-lactoside	280.5
pNP-β-D-maltoside	–
pNP-α-D-maltoside	–

A dash indicates that activity could not be detected. Derivatives with equatorial anomeric oxygen (assuming a $^4C_1$ conformation) are in bold.
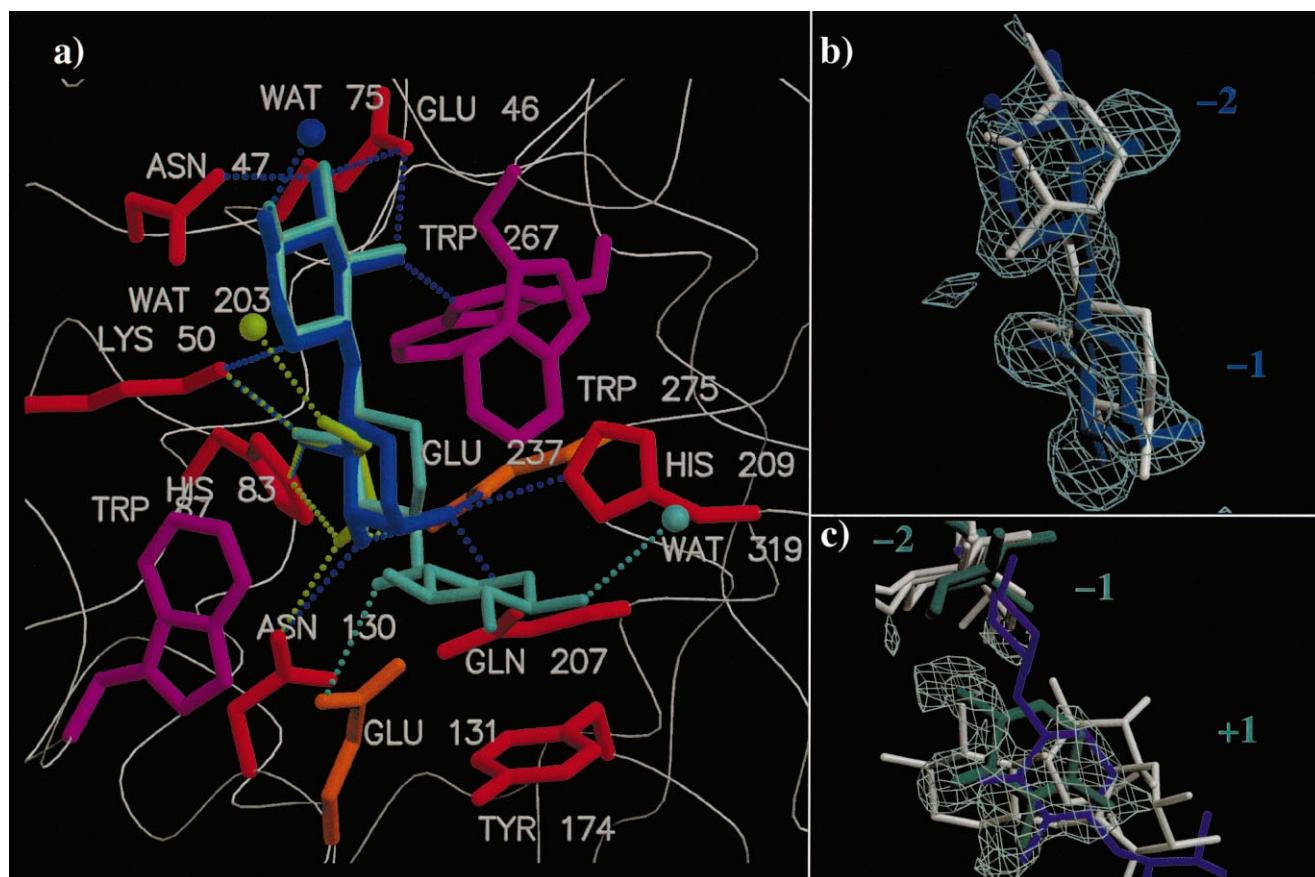
Fig. 1. Xylobiose and glycerol binding in TAX. TAX residues are shown for the XBCRYO structure in red, magenta (tryptophan residues forming the aromatic cage at subsite −1) or orange (catalytic glutamates). Xylobiose and water 75 in the XBCRYO structure is shown in blue. The sugar moieties occupying subsites −2, −1 and +1 in XBRT and water 319 are shown in cyan. Glycerol and water 203 from the GLC structure are shown in green. Potential hydrogen bonds with TAX (distances shorter than 3.2 Å) are coloured according to the same scheme as for the ligands. The substrate binding groove is oriented so that subsite −2 is at the top and subsite +1 is at the bottom. In panel b a Sigmaa $F_{obs}-F_{calc}$ map calculated prior to incorporation of xylobiose in the model (blue) is shown for XBCRYO contoured at 2σ around 1.5 Å from xylobiose. In white the conformation of xylobiose bound to the *P. simplicissimum* xylanase (PDB code 1B3W), is shown for comparison. In panel c a simulated annealing $2F_{obs}-F_{calc}$ omit map is shown for the xylose at subsite +1 in the XBRT model (cyan) contoured at 0.7σ. The complexes of *P. simplicissimum* xylanase with xylotetraose (PDB code 1B3Y) and xylopentaose (PDB code 1B3Z) are shown in white, and the complex of *P. fluorescens* xylanase 10A with xylopentaose (PDB code 1E5N) is shown in purple for comparison.

structure GLC. This is not unusual for carbohydrate-active enzymes, as glycerol can partly mimic substrate structure (for examples also in [34,35]). The O3 of glycerol is within hydrogen bonding distance of Asn 130 ND2, His 83 NE2 and Glu 237 OE2, while the O2 is within hydrogen-bonding distance of His 83 NE2 and Lys 50 NZ. Thus in this case the O2 of glycerol mimics the O3 of xylose at subsite −1, while glycerol O3 mimics xylose O2.

In the related *P. simplicissimum* xylanase [11] seven glycerol molecules originating from the cryoprotectant were included in the final model, but none in a position corresponding to the one found in TAX. This observation is surprising given the high conservation between TAX and *P. simplicissimum* xylanase at their active sites, and might also be related to the different experimental conditions. Thus structurally very similar xylanases can display different ligand binding modes locally, as already shown by the differences in xylooligosaccharide binding.

3.4. Complex formation with xylobiose stabilises Trp 275

Three residues at the active site, Trp 275 and the adjacent Arg 276 and Glu 46 (Fig. 2), adopt alternative conformations

of approximately equal populations (A and B) in crystal form II (1.14 Å resolution, PDB code 1GOK, 1K6A). As shown in Fig. 2, Trp 275A and Arg 276B are mutually exclusive. Water 203 (conserved in the GLC structure, Fig. 1a) is expelled if Trp 275 is in its B conformation. In addition to alternate conformations Trp 275 also has an average B factor (25.2 Å²) much higher than the average for the protein (12.6 Å²)
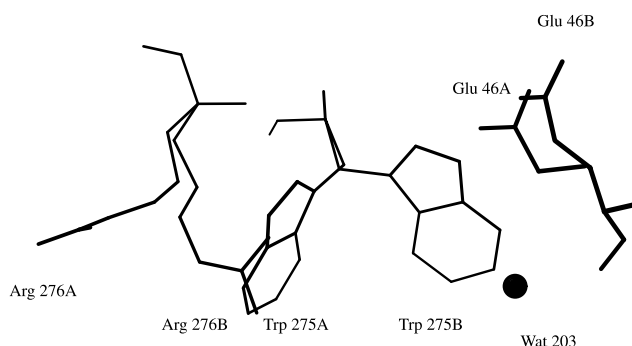

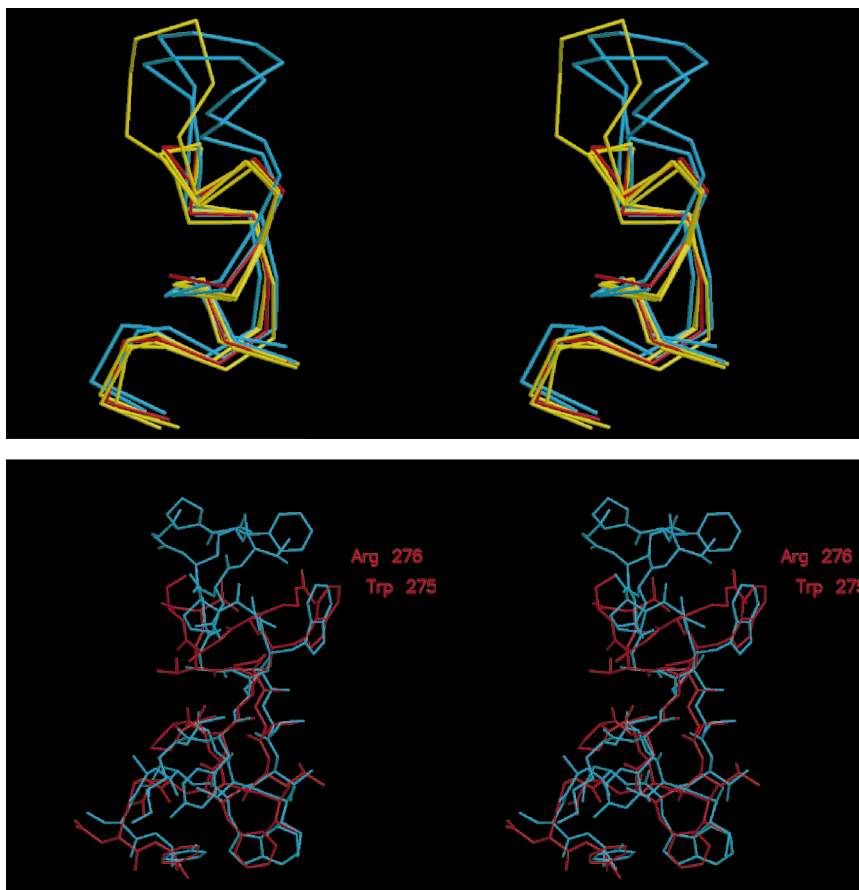Fig. 2. Alternative conformations for Glu 46, Trp 275 and Arg 276 in the form II crystal.

Fig. 3. Comparison of loop 8 structure in family 10 xylanases as (top) Cα trace and (bottom) full coordinates. In the top panel TAX is shown in red, the other subset 1 xylanases in yellow and the subset 2 xylanases in cyan. In the bottom panel TAX (red) is used as representative of subset 1, and CEX (blue) as a representative of subset 2.

and poor electron density, with a real space correlation coefficient calculated in CNS against a Sigmaa $2F_{obs}-F_{calc}$ map (RSCC) of 0.815, while the average RSCC per residue is 0.933 ± 0.029.

In the other uncomplexed structure available for TAX, obtained from crystal form I, the B conformation of Trp 275 is not obvious in the electron density maps perhaps due to the more limited resolution (1.92 Å), though there could be double conformations of Glu 46 and perhaps also of Arg 276. The A conformation of Trp 275 has a high average temperature factor, 30.1 Å^2 compared to the average 9.6 Å^2, and poor density also in this structure, with an RSCC of 0.861 compared to an average RSCC per residue of 0.935 ± 0.020. In contrast the electron density for Trp 275 is improved in the complexes with xylobiose. In the XBRT structure Trp 275 has an RSCC of 0.884, compared to an average RSCC per residue of 0.930 ± 0.026, while in the XBCRYO structure it has an RSCC of 0.948, compared to an average RSCC per residue of 0.953 ± 0.020. No B conformations can be detected for Trp 275, Arg 276 or Glu 46. Furthermore in the xylobiose complexes the B factors for Trp 275 (25.0 and 23.1 Å^2 for XBRT and XBCRYO, respectively) become closer to the average for the protein (17.3 and 18.0 Å^2 for XBRT and XBCRYO, respectively).

Reduced disorder for the residues equivalent to Trp 275 on complex formation with xylooligosaccharides has previously

been observed for *P. simplicissimum* xylanase 10A [28] and *P. fluorescens* xylanase 10A [32]. In the case of TAX we have an even more striking example as the B conformation disappears in the complex. TAX, *P. fluorescens* xylanase 10A and *P. simplicissimum* xylanase 10A are structurally similar in the eighth βα-loop region, where Trp 275 or its equivalent are situated (Fig. 3). The *Streptomyces lividans* and *Streptomyces olivaceoviridis* family 10 xylanases share this loop structure, while xylanase/exocellulase Cex from *Clostridium fimi* (CEX) and *Clostridium thermocellum* xylanase 10Z have an extra four-residue α-helical stretch immediately following the Trp (Fig. 3). Thus family 10 can be structurally divided into two subsets in which this helical stretch is either absent (subset 1) or present (subset 2).

In subset 2 the residue corresponding to Trp 275 in TAX can make extra hydrophobic/aromatic interactions with residues on the helical stretch (CEX Val 285 and Phe 286, xylanase 10Z Thr 807 and Phe 808, Fig. 3, bottom). B factor analysis shows that in subset 1 structures (PDB codes 2TAX, 1CLX, 1XYF, 1E0W and 1B31) the average ratio between average B factors of the equivalent residue of Trp 275 and the average B factors for the whole uncomplexed structures is 1.58, while for subset 2 (PDB codes 2EXO and 1XYZ) it is 1.19. This suggests that the residues corresponding to Trp 275 tend to be more disordered in uncomplexed subset 1 structures than in subset 2 structures.

4. Discussion

4.1. Structural basis of specificity

TAX kinetic parameters towards xylans are typical for family 10 xylanases [16,17,36]. TAX showed no activity on cellulosic substrates tested (CMC and Avicel), but had activity on pNP glucose derivatives. It has been suggested that shape recognition of the polysaccharide chain conformation [32,37] plays a role in polysaccharidase specificity. For family 10 xylanases this means the recognition of the three-fold helical conformation of xylan, as opposed to the flat ribbon-like conformation of cellulose, by a substrate binding groove that reflects the helical nature of the substrate. This observation might also explain TAX activity on barley glucan, in which β-1,3 linkages are present in addition to β-1,4 linkages, resulting in a more twisted conformation than cellulose.

Activity measurements against pNP substrates showed that only pNP-glycosides with equatorial pNP groups (see Table 2) could be hydrolysed. Hydrolysis of both pNP-α-L-arabinofuranoside and pNP-α-L-arabinopyranoside with similar specific activities shows that both a furanose and a pyranose ring can be accommodated at subsite −1. Both arabinoside derivatives were hydrolysed better than pNP-β-D-xylopyranoside and published kinetic parameters [38] show that the K_M of TAX is significantly lower for the arabinosides while the k_{cat} is higher for the xylopyranoside, suggesting that TAX has higher affinity for the arabinoside at subsite −1. The structures of the two monosaccharides are the same except that α-L-arabinopyranose has an axial hydroxyl at C4. Superimposing α-L-arabinopyranose onto xylose in the XBCRYO structure, it seems plausible that arabinose O4 could form an extra hydrogen bond to Lys 50 and/or Gln 90, explaining the increased affinity for TAX. The specific activities for pNP-β-D-galactose and pNP-β-D-glucose are similar, another example that the axial O4 does not impair the ability of TAX to bind a monomer at the −1 subsite.

pNP-glycosides of pentoses (xylose, arabinose) were hydrolysed better than pNP-glycosides of hexoses (glucose, galactose), and from the XBCRYO structure it is clear that an extra C6 interferes with Trp 275. The extra bulkiness at C6 in the pNP-β-D-glucuronide results in no activity towards this compound. The role of Trp 275 in specificity has been investigated by others [19,20] showing that the residues corresponding to TAX Trp 275 and Gln 90 in CEX and S. lividans xylanase 10A are displaced or become disordered if 2-fluorocellobioside is covalently bound to the enzyme, but not if 2-fluoroxylobiose is bound.

No hydrolysis of pNP-β-D-mannopyranoside could be detected. Mannose in a $^4C_1$ chair conformation has an axial hydroxyl at O2 as opposed to the equatorial O2 in xylose, which would clash with Trp 87, in addition to the C6 group clashing with Trp 275. The potential steric hindrance with two out of the three conserved Trp at subsite −1 would seem to prohibit binding.

As is to be expected for an endo-polysaccharidase, pNP β-1,4-linked disaccharide derivatives were hydrolysed better than pNP monosaccharide derivatives, even though they are disaccharides of hexose sugars which are not favoured at subsite −1. Binding at subsite −2 is likely to provide leverage for substrate distortion and catalysis at subsite −1, outweighing the cost of steric clashes with Trp 275. The lower activity for pNP-β-D-lactoside may be indicative that an axial hydroxyl at

C4 is not as easily accommodated at subsite −2 as it is at subsite −1. No activity was detected on pNP-maltosides, presumably because of the presence of an α-linkage.

4.2. Role of the eighth βα-loop in family 10 enzymes

According to our analysis of the eighth βα-loop of the barrel family 10 xylanases can be divided into two subsets on the basis of structure and Trp 275 mobility. This division does not mirror taxonomy, or overall divergence in sequences. At least one micro-organism, C. thermocellum, possesses a xylanase 10X [39] whose eighth βα-loop sequence and length suggest it belongs to subset 1, in addition to a subset 2 enzyme (xylanase 10Z). Thus it seems that xylanase sequences from the two subsets coexist in one genome, as do the structurally unrelated family 10 and 11 xylanases, suggesting that they might have subtly different roles.

Elucidation of these roles and the biochemical differences between the two subsets requires further investigation. It is tempting to propose that the mobility of Trp 275 in subset 1 enzymes means that the −1 subsite is not fully formed until stabilised by oligosaccharide binding, resulting in preference for longer oligosaccharides than subset 2 enzymes, which have a more rigid active site. A comparative study on P. fluorescens xylanase A and CEX [17], falling structurally in subsets 1 and 2 respectively, shows that CEX is indeed better at cleaving very short xylooligosaccharides.

4.3. Conclusions

Analysis of the structure of TAX in complex with xylobiose, coupled with a biochemical study with different sugar analogues, has allowed us to identify residues involved in the specificity for particular sugar substructures. A comparison with other family 10 structures revealed that a subset of this family has a mobile tryptophan on the eighth βα-loop, which becomes ordered and forms the −1 subsite on complex formation.

References

[1] Khandke, K.M., Vithayathil, P.J. and Murthy, S.K. (1989) Arch. Biochem. Biophys. 274, 491–500.
[2] Lo Leggio, L., Kalogiannis, S., Bhat, M.K. and Pickersgill, R.W. (1999) Proteins Struct. Funct. Genet. 36, 295–306.
[3] Teixeira, S., Lo Leggio, L., Pickersgill, R. and Cardin, C. (2001) Acta Crystallogr. D57, 385–392.
[4] Natesh, R., Bhanumoorthy, P., Vithayathil, P.J., Sekar, R., Ramakumar, S. and Viswamitra, M.A. (1999) J. Mol. Biol. 288, 999–1012.
[5] Coutinho, P.M. and Henrissat, B. (1999) In: Recent Advances in Carbohydrate Bioengineering, The Royal Society of Chemistry, London, pp. 3–12.
[6] Harris, G.W., Jenkins, J.A., Connerton, I., Cummings, N., Lo Leggio, L., Scott, M., Hazlewood, G.P., Laurie, J.I., Gilbert, H.J. and Pickersgill, R.W. (1994) Structure 2, 1107–1116.
[7] Harris, G.W., Jenkins, J.A., Connerton, I. and Pickersgill, R.W. (1996) Acta Crystallogr. D52, 393–401.
[8] Derewenda, U., Swenson, L., Green, R., Wei, Y., Morosoli, R.,

Shareck, F., Kluepfel, D. and Derewenda, Z.S. (1994) J. Biol. Chem. 33, 20811–20814.

[9] White, A., Withers, S.G., Gilkes, N.R. and Rose, D.R. (1994) Biochemistry 33, 12546–12552.

[10] Dominguez, R., Souchon, H., Spinelli, S., Dauter, Z., Wilson, K.S., Chauvaux, S., Béguin, P. and Alzari, P.M. (1995) Nature Struct. Biol. 2, 569–576.

[11] Schmidt, A., Schlacher, A., Steiner, W., Schwab, H. and Kratky, C. (1998) Protein Sci. 7, 2081–2088.

[12] Fujimoto, Z., Kuno, A., Kaneko, S., Yoshida, S., Kobayashi, H., Kusakabe, I. and Mizuno, H. (2000) J. Mol. Biol. 300, 575–585.

[13] Jenkins, J., Lo Leggio, L., Harris, G. and Pickersgill, R.W. (1995) FEBS Lett. 362, 281–285.

[14] Henrissat, B., Callebaut, I., Fabrega, S., Lehn, P., Mornon, J.-P. and Davies, G. (1995) Proc. Natl. Acad. Sci. USA 92, 7090–7094.

[15] Davies, G. and Henrissat, B. (1995) Structure 3, 853–859.

[16] Roberge, M., Shareck, F., Morosoli, R., Kluepfel, D. and Dupont, C. (1999) Protein Eng. 12, 251–257.

[17] Charnock, S.J., Spurway, T.D., Xie, H., Beylot, M.-H., Virden, R., Warren, R.A.J., Hazlewood, G.P. and Gilbert, H.J. (1998) J. Biol. Chem. 273, 32187–32199.

[18] Charnock, S.J. (1998) Structure/function Analysis of a Family 10 Glycosyl Hydrolase, PhD Thesis, University of Newcastle.

[19] Notenboom, V., Birsan, C., Warren, R.A.J., Withers, S.G. and Rose, D.R. (1998) Biochemistry 37, 4751–4758.

[20] Ducros, V., Charnock, S., Derewenda, U., Derewenda, Z., Dauter, Z., Dupont, C., Shareck, F., Morosoli, R., Kluepfel, D. and Davies, G. (2000) J. Biol. Chem. 275, 23020–23026.

[21] Kalogiannis, S., Owen, E., Beever, D.E. and Bhat, M.K. (1995) Med. Fac. Landbouwwet. Univ. Gent 60, 1995–1998.

[22] Bailey, M.J., Biely, P. and Poutanen, K. (1992) J. Biotechnol. 23, 257–270.

[23] Otwinoski, Z. and Minor, W. (1997) Methods Enzymol. 276, 307–326.

[24] Brunger, A.T., Kuryjian, J. and Karplus, M. (1987) Science 235, 458–460.

[25] Brunger, A.T., Adams, P.D., Clore, G.M., DeLano, W.L., Gros, P., Grosse-Kunstleve, R.W., Jiang, J.S., Kuszewski, J., Nilges, M., Pannu, N.S., Read, R.J., Rice, L.M., Simonson, T. and Warren, G.L. (1998) Acta Crystallogr. D54, 905–921.

[26] Jones, T.A., Zou, J.Y., Cowan, S.W. and Kjeldgaard, M. (1991) Acta Crystallogr. A47, 110–119.

[27] Davies, G.J., Wilson, K.S. and Henrissat, B. (1997) Biochem. J. 321, 557–559.

[28] Schmidt, A., Gábitz, G.M. and Kratky, C. (1999) Biochemistry 38, 2403–2412.

[29] Davies, G.J., Dauter, M., Brzozowski, A.M., Bjørnvad, M.E., Andersen, K.V. and Schhlein, M. (1998) Biochemistry 37, 1926–1932.

[30] Notenboom, V., Birsan, C., Nitz, M., Rose, D.R., Warren, R.A.J. and Withers, S.G. (1998) Nature Struct. Biol. 5, 812–818.

[31] White, A., Tull, D., Johns, K., Withers, S. and Rose, D.R. (1996) Nature Struct. Biol. 3, 149–154.

[32] Lo Leggio, L., Jenkins, J., Harris, G.W. and Pickersgill, R.W. (2000) Proteins 41, 362–373.

[33] Notenboom, V., Williams, S.J., Hoos, R., Withers, S.G. and Rose, D.R. (2000) Biochemistry 39, 11553–11563.

[34] Burmeister, W.P., Cottaz, S., Rollin, P., Vasella, A. and Henrissat, B. (2000) J. Biol. Chem. 275, 39385–39393.

[35] Varrot, A., Hastrup, S., Schhlein, M. and Davies, G.J. (1999) Biochem. J. 337, 297–304.

[36] Charnock, S., Lakey, J., Virden, R., Hughes, N., Sinnott, M., Hazlewood, G.P., Pickersgill, R. and Gilbert, H.J. (1997) J. Biol. Chem. 272, 2942–2951.

[37] Hrmova, M. and Fincher, G. (2001) Plant Physiol. 125, 54–57.

[38] Kalogeris, E., Christakopoulos, P., Vršanská, M., Kekos, D., Biely, P. and Macris, B.J. (2001) J. Mol. Catal. B 11, 491–501.

[39] Kim, H., Jung, K.H. and Pack, M.Y. (2000) Appl. Microbiol. Biotechnol. 54, 521–527.